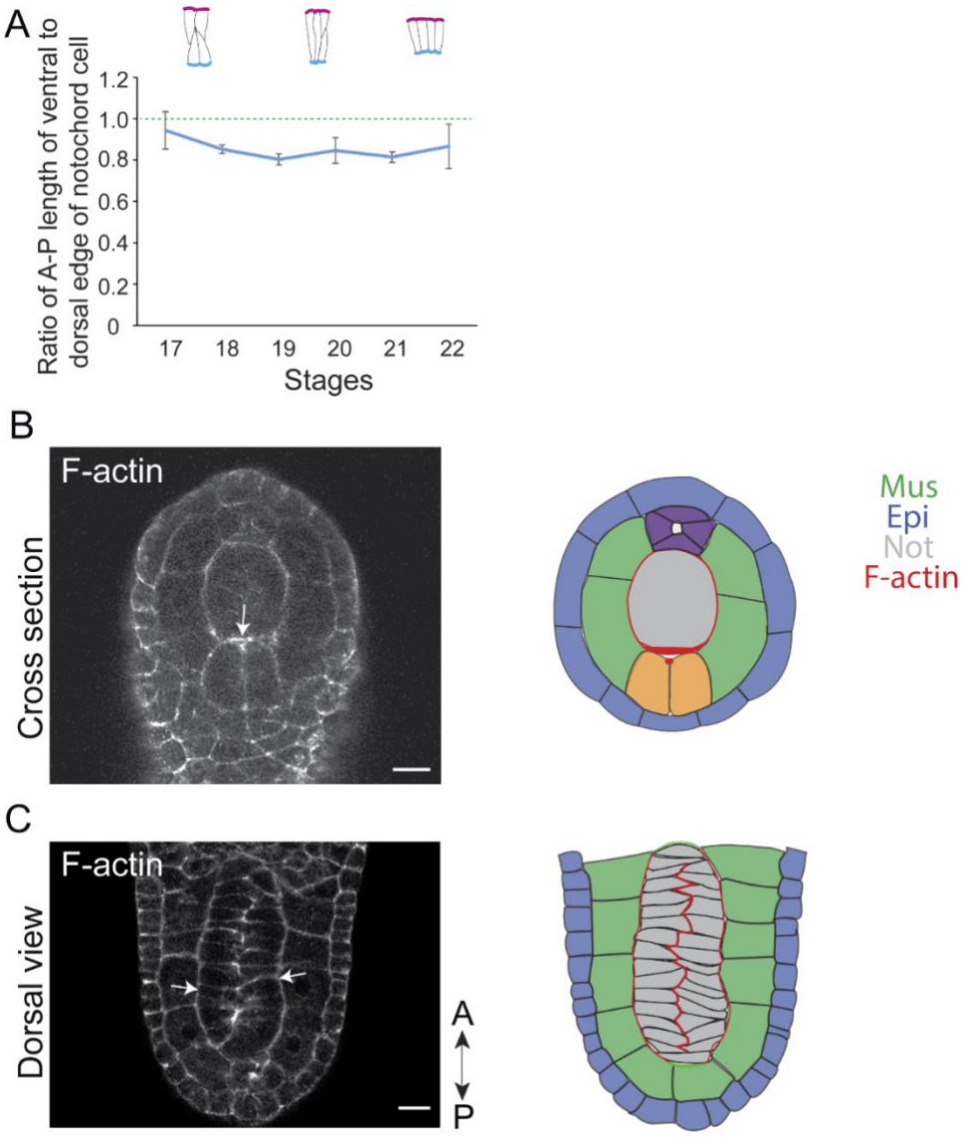

Fig. S1. The notochordal cells' geometry and F-actin in *Ciona* notochord. Related to Fig. 2. (A) Changes in notochordal cells' geometry by measuring the ratios of A-P length at dorsal and ventral edge of notochord cells in embryos at tailbud stages 17–22. Insets: notochordal cell shapes at tailbud stages 17, 19, and 21. Ratio = 1 is marked by a green dashed line. (B) Axial section of the notochord (left), highlighted in the drawings (right). Enriched F-actin at the notochord's ventral side (white arrows). Scale bar = 10 μm. (C) Dorsal view of the notochord (left). Both left and right sides of the notochord (indicated by arrows) have relatively the same level of F-actin, summarized in the drawings (right). Scale bar = 10 μm.

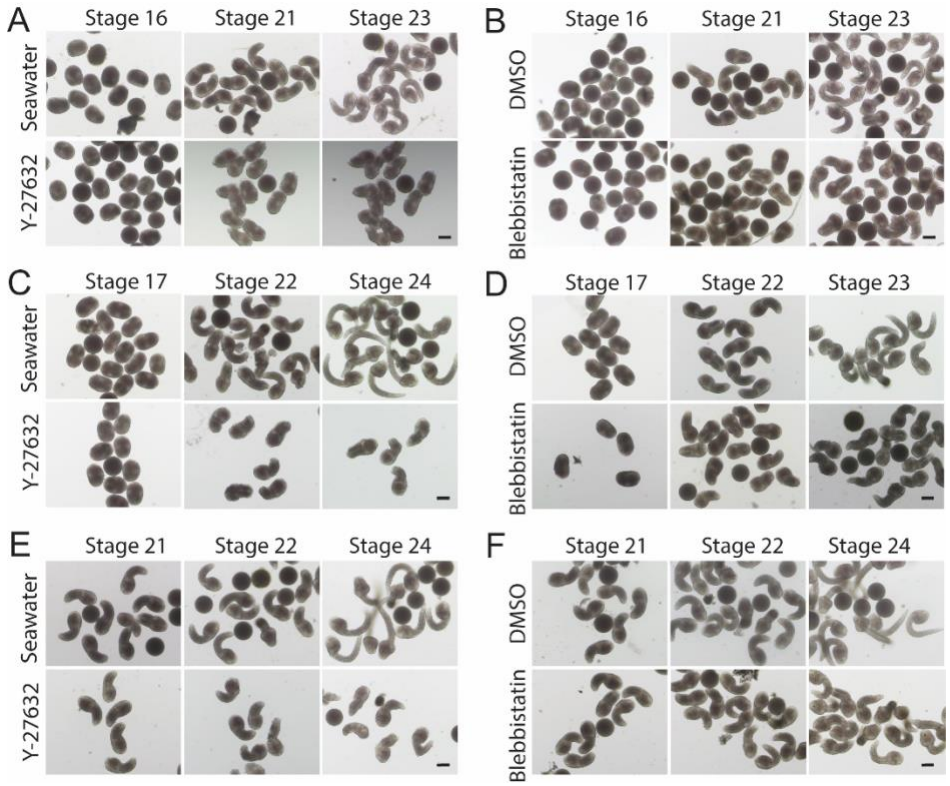

Fig. S2. Effects of drug treatment on embryonic tail bending in *Ciona robusta*. (A) Embryos' morphology before (left panel) and after the treatment with 200 µM Y-27632 or seawater (control). Treatment started at tailbud stage 16 (16°C). Scale bar = 100 µm. (B) Embryos' morphology before (left panel) and after the treatment with 100 µM blebbistatin or DMSO (control). Treatment was started at tailbud stage 16 (16 °C). Scale bar = 100 µm. (C) Embryos' morphology before (left panel) and after the treatment with 200 µM Y-27632 or seawater (control). Treatment started at tailbud stage 17 (16°C). Scale bar = 100 µm. (D) Embryos' morphology before (left panel) and after the treatment with 100 µM blebbistatin or DMSO (control). Treatment started at tailbud stage 17 (16 °C). Scale bar = 100 µm. (E) Embryos' morphology before (left panel) and after the treatment with 200 µM Y-27632 or seawater (control). Treatment started at tailbud stage 21 (16°C). Scale bar = 100 µm. (F) Embryos' morphology before (left panel) and after the treatment with 100 µM blebbistatin or DMSO (control). Treatment started at tailbud stage 21 (16 °C). Scale bar = 100 µm.

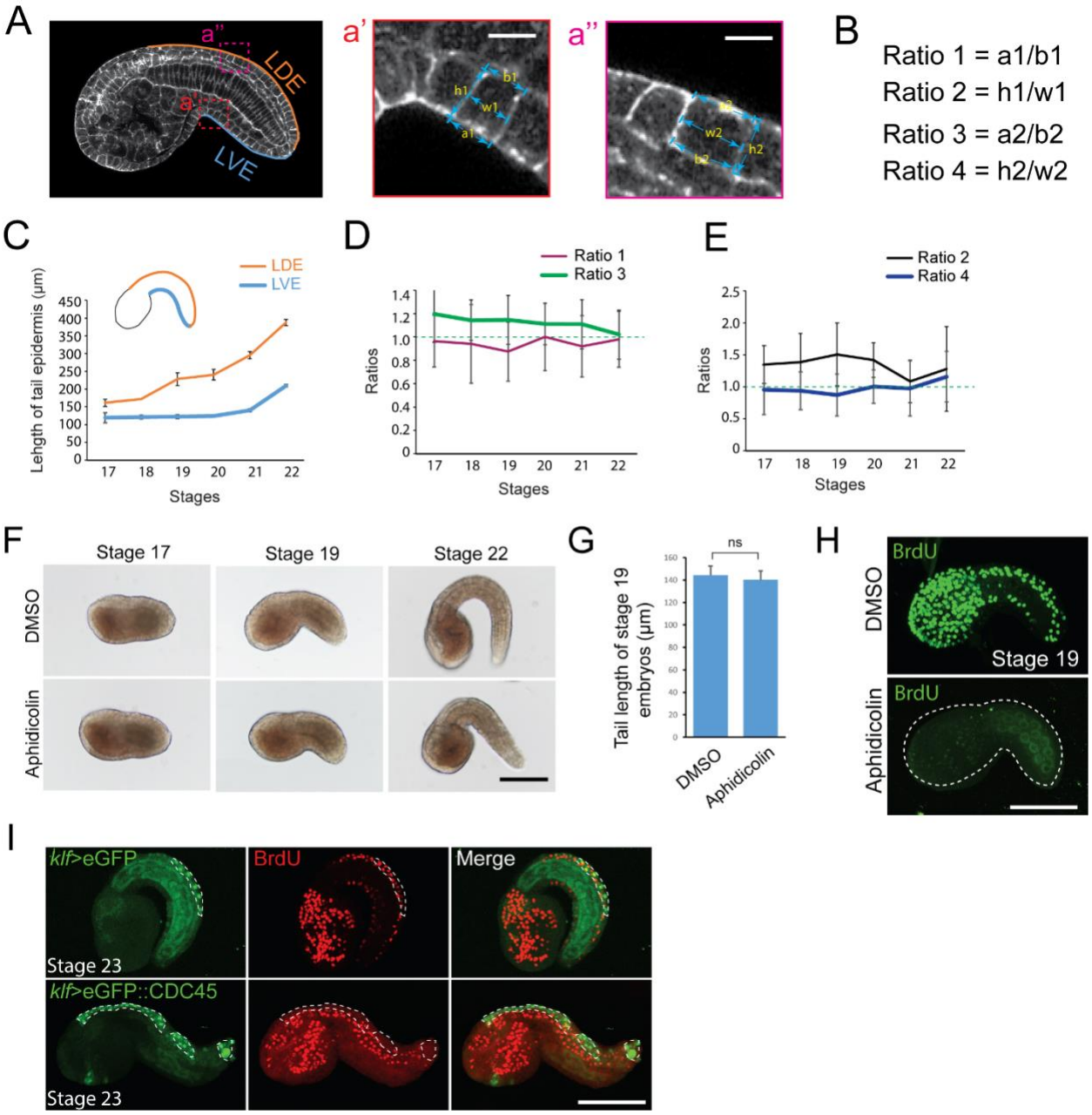

Fig. S3. Characterization of the role of epidermis during the embryonic tail bending in *Ciona robusta*. Related to Fig. 4. (A) Quantification of tail epidermal cell geometry in the basis of the confocal images. The embryos were stained by phalloidin. LDE, length of dorsal edge of embryo tail; LVE, length of ventral edge of embryo tail. Higher-magnification images of red- (a') and magenta-dashed (a'') box area. Scale bar = 10 µm. (B) Definition of ratios that describing the tail epidermis geometry (the corresponding

parameters are referred to A). (C) Changes in dorsal and ventral length of tail epidermis at tailbud stages 17–22. (D) Changes in ratios 1 and 3 at tailbud stages 17–22. Ratio = 1 is marked by a green dashed line. (E) Changes in ratios 2 and 4 at tailbud stages 17–22. Ratio = 1 is highlighted by a green dashed line. (F) DIC images displaying morphologies of DMSO- or aphidicolin-treated embryos at tailbud stages 17, 19, and 22. (G) Quantification of tail length of DMSO- (n = 31) or aphidicolin-treated (n=31) embryos at tailbud stage 19. (H) Confocal images (projection) showing distribution of BrdU-positive cells in DMSO- or aphidicolin-treated embryos at tailbud stage 17, 19, and 23. Scale bar = 100 μm. (I) Confocal images (projection) showing distribution of BrdU-positive cells in *klf*>eGFP- and *klf*>eGFP∷cdc45- transfected embryos at tailbud stage 23. eGFP driven by *klf* promoter is expressed along the dorsal midline of epidermis (white dashed lines). Scale bar = 100 μm.

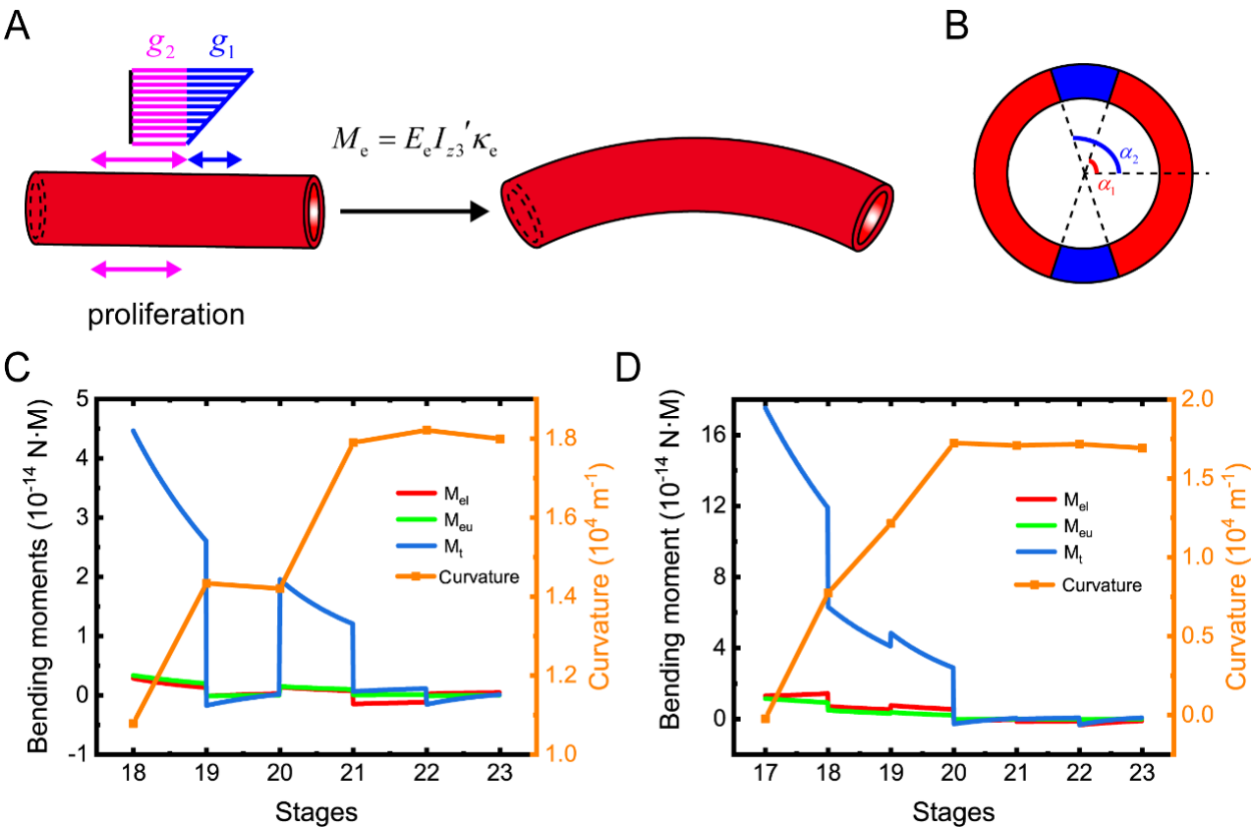

Fig. S4. Physical model for evaluating the contributions of notochord and epidermis during tail bending. (A) Gradient growth is used to simulate the volume change caused by differential epidermis proliferation. The growth of the epidermis can be divided into two parts, the differential part g_1 and the uniform part g_2. (B) The cross section of the epidermis. The blue parts represent the dorsal and ventral epidermal cells undergoing mitosis. α_2 and α_1 are the polar coordinates of the cell boundaries. (C) and (D) show the bending moments induced by epidermis cell division, M_{el} and M_{eu}, and the total moment required to bend the tail for two typical embryos, M_{t}. The evolution of the curvature of the tail is also shown in (C) and (D).

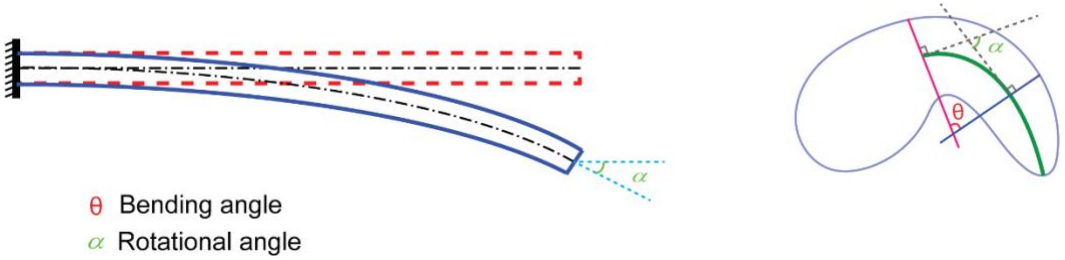

Fig. S5. The rotational and bending angle. The diagrams illustrate the definition of the rotational angle *α* and its relationship with bending angle *θ*.

Supplementary Materials and Methods

Physical model

To quantify the contribution of the notochord and epidermis to the tail bending, we proposed a composite beam model considering active processes (e.g., differential epidermis proliferation and notochord constriction) in the tail. The tail was theoretically treated as a cylindrical beam comprising three layers representing, from inside to outside, the notochord, muscle, and epidermis, respectively.

As the tail bends, dorsal epidermal cells proliferate faster than ventral ones. The effects of differential cell divisions may be divided into two portions: cell divisions may enlarge the total volume of the epidermis and further bend the tail; and cell divisions along the anteroposterior (AP) axis may actively elongate the cells along the AP axis, shortening the cell width correspondingly.

First, we evaluated the effect of cell volumes enlargement. In this case, we neglected the possibility that cell divisions along the AP axis may actively elongate the cells along the AP axis. Gradient growth was used to simulate the volume change caused by differential epidermis proliferation, as shown in Fig. S4A. Epidermis growth expansion was restricted to the axial direction. The growth of the epidermis can be divided into two parts, the differential part g_1 and the uniform part g_2. The differential growth strain, denoted by g_1, induces a spontaneous curvature

$$\kappa_e = \frac{g_1}{d_3}. \tag{S1}$$

As the epidermis proliferates, the restraint by the notochord and muscle can create a relatively high stress in the tail. The bending moment M_e due to the differential proliferation of the epidermis can be calculated by

$$M_e = E_e I_{z3}' \kappa_e, \tag{S2}$$

where I'_{z3} is the moment of inertia for the dorsal and ventral epidermis undergoing differential cell division and is given by

$$I'_{z3} = \frac{d_3^4 - d_2^4}{64}\left(\alpha_2 - \alpha_1 - \frac{\sin 2\alpha_2 - \sin 2\alpha_1}{2}\right), \quad \text{(S3)}$$

where α_2 and α_1 are the polar coordinates of the cell boundaries, as shown in Fig. S4B. Substituting Eqs. (S1) and (S3) into Eq. (S2), we get

$$M_e = \frac{d_3^4 - d_2^4}{32 d_3}\left(\frac{\alpha_2 - \alpha_1}{2} - \frac{\sin 2\alpha_2 - \sin 2\alpha_1}{4}\right) E_e g_1. \quad \text{(S4)}$$

where g_1 is the amount of differential tissue growth. According to the volume growth theory, g_1 is given by

$$g_1 = \frac{\Delta L_e}{L}, \quad \text{(S5)}$$

where ΔL_e is the differential length between the dorsal and ventral sides of the epidermis because of differential epidermis proliferation. The observed differential length between the dorsal and ventral sides of the epidermis, ΔL_{em}, is due to both epidermis differential proliferation and notochord constriction. The observed differential length ΔL_{em} can be divided into two parts: the differential length $\Delta L'_e$ due to elastic deformation (the contraction of the notochord) and the differential length ΔL_e due to differential proliferation, $\Delta L_{em} = \Delta L_e + \Delta L'_e$. $\Delta L'_e$ can be obtained as follows. First, when the epidermis proliferation is neglected, the epidermis is assumed as incompressible and the volume of epidermis is conserved for different stages. Then, we can calculate the change of length $\Delta L'_e$ from the changes in the epidermis height and width measured from experiments. Substituting ΔL_e into Eq. (S5) and then into Eq. (S4), we obtain the contribution of differential cell divisions due to the change of volume, M_{el}.

Secondly, we considered the condition that cell divisions along the AP axis may actively elongate the cells along the AP axis and thus bend the tail. During the tail bending, the elongation of the notochord may also stretch and elongate the epidermal cells along the AP axis. Therefore, it is hard to distinguish the contributions of these two mechanisms to the length change. In this part, we considered an extreme situation: the elongation of the epidermis along the AP axis is totally caused by cell division, i.e., the notochord does not stretch the epidermis. In this vein, the observed differential length ΔL_{em} is fully caused by differential cell divisions. Substituting ΔL_{em} into Eq. (S5) and then into Eq. (S4), we obtain an estimate of the contribution of differential cell divisions, M_{eu}.

During embryonic tail bending, F-actin and myosin II asymmetrically assemble at the notochord's ventral side, causing notochord constriction. The bending moment produced by the contractile force M_{n} is hard to calculate directly, since the underlying mechanisms of actomyosin constriction are complex and difficult to measure. Therefore, an indirect approach is utilized. First, the total moment required to bend the whole tail is calculated as

$$M_{\mathrm{t}} = EI_{\mathrm{z}}\kappa_{\mathrm{t}}, \tag{S6}$$

where EI_{z} is the bending stiffness of the tail and is given by

$$EI_{\mathrm{z}} = \frac{E_{\mathrm{n}}\pi d_1^4}{64} + \frac{E_{\mathrm{m}}\pi d_2^4}{64}\left(1-\frac{d_1^4}{d_2^4}\right) + \frac{E_{\mathrm{e}}\pi d_3^4}{64}\left(1-\frac{d_2^4}{d_3^4}\right), \tag{S7}$$

where E_{m} and E_{e} are Young's modulus of the muscle and epidermis, respectively; I_Z is the moment of inertia; and κ_{t} is the curvature of the tail. Then the bending moment caused by the contraction of notochord M_{n} can be calculated by $M_{\mathrm{n}} = M_{\mathrm{t}} - M_{\mathrm{e}}$.

Using the representative values of the parameters given in Fig. 5 and Table S1, the bending moments M_{el}, M_{eu} and M_t were calculated for different stages for two typical embryos (Figs. S4C,D). The curvatures of the tail were calculated to depict the bending process. It is shown that at tailbud stages ~17–20/21 the curvature increases and the tail bends gradually, while at the tailbud stages ~20/21–23 the curvature is almost unchanged and the tail does not bend further, though the length of the tail continues to increase. Accordingly, the total moment M_t is positive for the early stages, while M_t falls to close to zero at the late stages. It is shown that the bending moment induced by the differential cell division of epidermis, M_{el} and M_{eu}, is relatively tiny compared to the total bending moment M_t. In this vein, we concluded that the contribution of the epidermis to the tail bending is dispensable, which is also confirmed by our experiments.

It was worth to note that in the above calculations, the geometric parameters of the same embryo for different stages were used. The precise values of the geometric parameters are difficult to obtain, therefore the DIC images of the embryo are used which may lead to some errors of the data. Though the value of the bending moments may be not quite accurate, the underlying mechanisms are conserved. Furthermore, the results show that the bending moment caused by the differential epithelial proliferation is pretty small, we believe that the limited errors of the data cannot change the conclusion that the contribution of epithelial proliferation is dispensable.

Table S1. Geometric measurements of the staged 17–22 *Ciona* embryos.

	Items	Stage 17	Stage 18	Stage 19	Stage 20	Stage 21	Stage 22
Embryo	A-P length of the embryo	215.87 ± 9.50	230.84 ± 7.94	277.86 ± 10.10	287.37 ± 12.53	330.93 ± 22.53	397.18 ± 19.25
	A-P length of the tail	126.42 ± 5.36	135.73 ± 9.12	170.02 ± 2.17	181.59 ± 10.71	221.99 ± 6.43	277.07 ± 26.84
Notochord	A-P length of the dorsal edge of the notochord	121.29 ± 6.21	143.06 ± 6.83	165.21 ± 1.72	186.31 ± 14.52	235.68 ± 12.84	283.28 ± 25.28
	Average diameter of the spherical notochord	--	38.43 ± 4.36	36.14 ± 5.94	31.22 ± 4.79	27.00 ± 1.16	23.98 ± 3.30
	Number of notochordal cell occupied along the dorsal edge of notochord	~18	~22	~27	~35	40	40
	A-P length of the ventral edge of the notochord	106.42 ± 11.09	116.87 ± 12.29	131.79 ± 12.30	147.51 ± 18.02	181.98 ± 11.87	245.49 ± 29.87
	Number of notochordal cell occupied along the ventral edge of notochord	~17	~21	~27	~33	40	40
	Average A-P length of notochord cell (along the dorsal edge)	6.51 ± 0.53	6.44 ± 0.65	6.15 ± 1.19	5.25 ± 0.34	6.06 ± 0.77	7.60 ± 0.79
	Average A-P length of notochord cell (along the ventral edge)	6.11 ± 0.41	5.40 ± 0.51	4.93 ± 0.91	4.44 ± 0.41	4.93 ± 0.67	6.59 ± 1.21
Tail epidermis	A-P length of dorsal midline of tail epidermis	161.41 ± 10.58	172.26 ± 0.46	228.20 ± 17.63	240.50 ± 14.72	295.32 ± 22	387.06 ± 39.26
	Average A-P length of dorsal midline of tail epidermal cell （apical domain ）	13.623 ± 3.82	10.60 ± 2.23	11.72 ± 2.86	9.66 ± 1.66	9.92 ± 2.46	8.62 ± 2.3
	Average D-V length of dorsal midline of tail epidermal cell	12.06 ± 3.24	10.84 ± 1.77	9.35 ± 2.43	9.09 ± 1.92	8.56 ± 1.98	9.01 ± 1.73
	Cell number of dorsal midlines of tail epidermis (section)	~ 11	~ 17	~ 20	~ 28	~ 38	~ 45
	A-P length of ventral midline of tail epidermis	119.53 ± 14.13	121.24 ± 5.70	122.48 ± 5.06	123.86 ± 0.63	140.45 ± 8.81	209.51 ± 40.81
	Average A-P length of ventral midline of tail epidermal cell (apical domain)	10.52 ± 2.54	9.54 ± 3.66	6.9 ± 2.4	7.63 ± 2.11	8.28 ± 1.56	6.96 ± 3.06
	Average D-V length of ventral midline of tail epidermal cell	14.33 ± 2.94	12.92 ± 2.28	10.84 ± 1.68	10.96 ± 1.26	9.22 ± 1.22	9.61 ± 1.79
	Cell number of ventral midlines of tail epidermis (section)	~ 10	~ 12	~ 16	~ 16	~ 20	~ 30

Movie 1. Time-lapse movie shows the development of *Ciona* embryo within chorion.

Movie duration is for 2.72 h, and is shown at 100 frames per second. Shown as stills in Fig. 1A. Scale bar = 50 μm.

Movie 2. Time-lapse movie shows the development of the dechorionated *Ciona* embryo.

Movie duration is for 1.75 h, and is shown at 100 frames per second. Shown as stills in Fig. 1A. Scale bar = 50 μm.

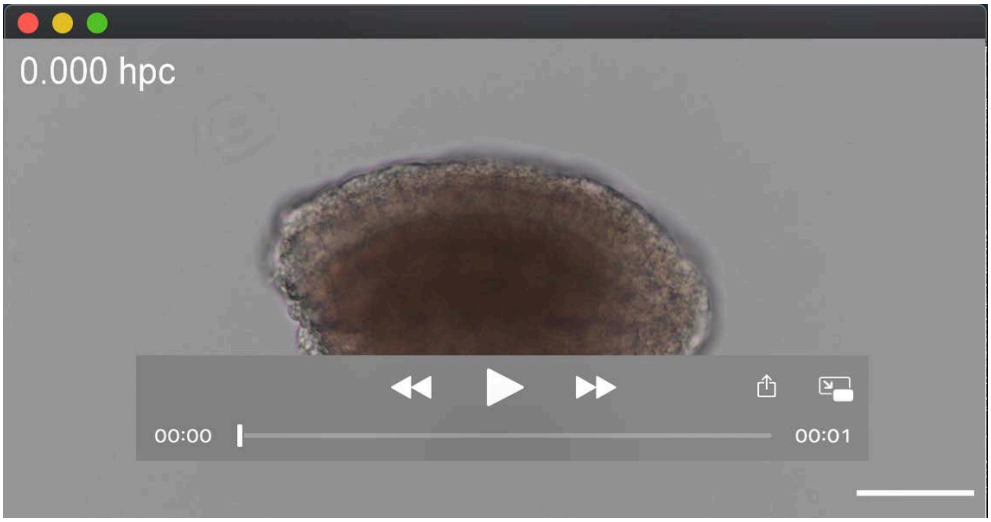

Movie 3. Time-lapse movie shows the development of the cutting tail.

Movie duration is for 1.91 h, and is shown at 100 frames per second. Shown as stills in Fig. 1D. Scale bar = 50 μm.

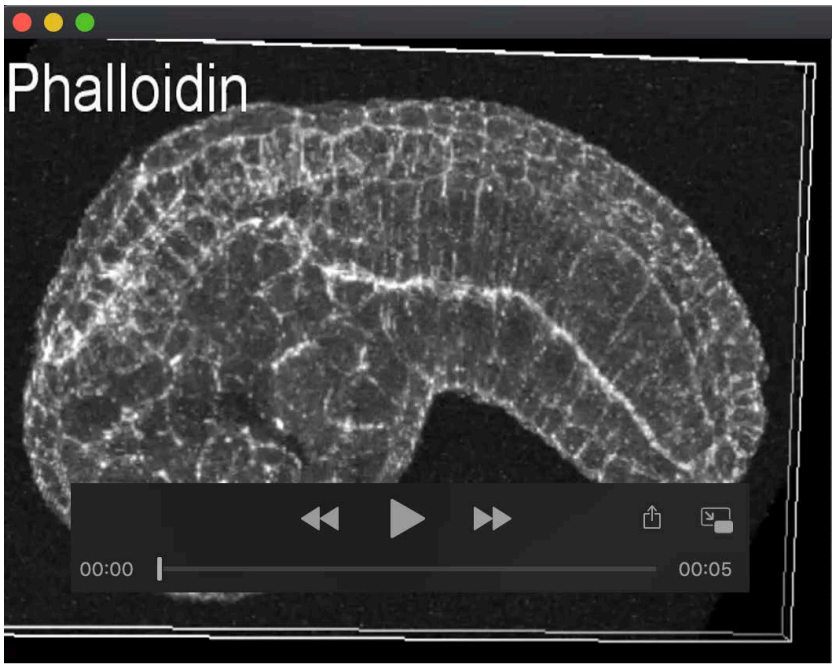

Movie 4. 3D rendering movie from confocal image of the phalloidin-stained embryo at tailbud stage 19.

Embryo is stained with 1/200 Alexa Fluor® 488-conjugated phalloidin.

Movie 5. 3D rendering movie from confocal images of the BrdU-stained embryo at tailbud stage 19.

BrdU-positive cells (green) are merged with DIC image of the same embryo.